JOURNAL OF THERMOPHYSICS AND HEAT TRANSFER
Vol. 21, No. 3, July–September 2007

Convective Droplet Impact and Heat Transfer from a NACA Airfoil

X. Wang*
University of Manitoba, Winnipeg, Manitoba R3T 5V6, Canada
G. F. Naterer†
University of Ontario Institute of Technology, Oshawa, Ontario L1H 7K4, Canada
and
E. Bibeau‡
University of Manitoba, Winnipeg, Manitoba R3T 5V6, Canada

DOI: 10.2514/1.27850

This paper develops a new nondimensional correlation of convective heat transfer with impinging droplets on a NACA airfoil. Both average and local Nusselt numbers are determined in terms of the Reynolds number, Prandtl number, and liquid water content of the droplet flowfield. A new multiphase Reynolds parameter is developed to normalize the experimental data, along a curve fit to measured data over a range of flow conditions. In this way, a modified Hilpert correlation can be extended to include effects of droplet–air interactions on the effective heat transfer coefficient. Droplet impact on the airfoil surface affects the structure of the thermal boundary layer, as well as energy exchange through kinetic energy of impinging droplets and a thin flowing film along the surface. Using the empirical correlation with a multiphase Reynolds parameter, this paper demonstrates that effects of varying both air velocity and liquid water content can be normalized into a single modified Hilpert correlation. Results are presented at varying Reynolds numbers and applications to icing problems are discussed.

Nomenclature

c	=	chord of airfoil, m
$\bar{h}$	=	average heat transfer coefficient, W/m^2K
h_i	=	local convective heat transfer coefficient, W/m^2K
k	=	thermal conductivity, W/mK
$\overline{Nu}$	=	average Nusselt number
Nu_x	=	local Nusselt number
Pr	=	Prandtl number
Re_c	=	Reynolds number, based on a chord reference length
T_{in}	=	inner surface temperature of airfoil, °C
T_o	=	outer surface temperature of airfoil, °C
T_∞	=	freestream temperature, °C
W	=	nondimensional liquid water content
δ	=	thickness of airfoil, m
ρ	=	density of air, kg/m^3
μ	=	dynamic viscosity of air, kg/ms

I. Introduction

CONVECTIVE heat transfer with impinging droplets on a surface occurs in numerous technological problems, ranging from icing of aircraft, to thermal spray coatings and advanced cooling systems. Heat transfer during droplet impact is a two-phase process involving droplet–air interactions. Icing of aircraft surfaces, wind turbine blades, and other structures is highly dependent on convective droplet impact. The droplets impart kinetic energy, latent heat of phase change, and a thin flowing film along the surface, which alters the thermal boundary layer (Messinger [1], Naterer [2,3]). Past studies have applied both Lagrangian [4,5] and Eulerian methods [6] to droplet tracking in icing problems. Empirical coefficients of convective heat transfer are often needed, but limited experimental data are available to support convection models with impinging droplets. This paper presents new experimental data to correlate heat transfer coefficients with liquid water content in droplet flows. The data can provide useful input for icing problems involving aircraft, wind turbine blades, and other airfoil applications.

Numerous past studies have been conducted for empirical correlations of forced convection heat transfer from cylinders, plates, and other geometrical configurations without impinging droplets. For basic configurations such as a flat plate, analytical expressions can be developed for the Nusselt number, in terms of Reynolds and Prandtl numbers. However, empirical correlations based on experimental data are generally required for most bluff bodies in external flow. A standard functional form for these correlations involves a product of Reynolds and Prandtl numbers, raised to exponents that depend on various factors, including flow conditions and geometrical configurations [7]. This paper correlates experimental data into this standard functional form, with a dependence on the liquid water content.

Common geometrical configurations of past droplet flow studies include impinging water droplets on cables, airfoils, and cylinders. Fortin et al. [8] developed a predictive model of heat transfer during droplet impact and ice accretion on an airfoil surface. Surface runoff of impinging droplets depends on the temperature gradient within the flowing surface film (Naterer [9]). Fu et al. [10] developed a two-dimensional icing model to simulate the process of ice accretion on overhead power line cables. The water droplet trajectory, film thickness and direction, local collision efficiency and local heat transfer coefficient were computed. Also, the authors analyzed the thermal boundary layer to calculate the convective heat transfer, unlike this paper which uses heat conduction within the wall to infer convection rates external to the surface. The past studies predicted the ice shape and weight over various configurations and cylinders,

Received 15 September 2006; revision received 23 December 2006; accepted for publication 25 January 2007.

*Ph.D. Candidate, Department of Mechanical and Manufacturing Engineering, University of Manitoba, Winnipeg, Manitoba R3T 5V6, Canada.

†Professor and Director of Research, Graduate Studies and Development, Faculty of Engineering and Applied Science, University of Ontario Institute of Technology, 2000 Simcoe Street North, Oshawa, Ontario L1H 7K4, Canada.

‡Natural Sciences and Engineering Research Council of Canada/Manitoba Hydro Alternative Energy Industrial Chair, Department of Mechanical and Manufacturing Engineering, University of Manitoba, Winnipeg, Manitoba R3T 5V6, Canada.

whereas this article focuses on heat transfer from a NACA airfoil. The predicted ice shapes were presented for a range of flow conditions. Ge and Fan [11] simulated the impact of subcooled water and *n*-heptane droplets on a superheated flat surface, specifically to investigate the detailed fluid dynamic behavior of the impacted droplets. Phase change heat transfer and droplet dynamics were compared against experimental data. Naterer and Camberos [12] reviewed the significance of entropy transport and the Second Law, when analyzing processes of phase change heat transfer. This article specifically examines heat transfer of impinging droplets without freezing and ice formation. The correlations can be incorporated into the convective component of energy balances at the surface, in combination with additional modes that would include the latent heat of phase change, if icing predictions were performed. Unlike past studies of convective heat transfer without droplets, this article develops correlations for conditions with impacting droplets on a NACA airfoil.

Various past studies have acquired experimental data involving droplet impact and heat transfer. Hedrih et al. [13] investigated the distribution of water droplets with an ultrasound sprayer. The density distribution function was presented with experimental data. The density distribution and liquid water content (LWC) are key meteorological parameters that affect the ice accretion on aircraft surfaces (Fuchs and Schickel [14]). Yoon et al. [15] investigated the flow of water droplets over cylinders, both heated and unheated. Five K-type thermocouples and heaters were assembled into an aluminum cylinder with a diameter of 29.2 mm and a length of 305 mm. Phase Doppler interferometry was used to measure the droplet mean size and velocity, downstream of the cylinder. Predicted and measured results showed good agreement in terms of the mean droplet size and velocity distribution. Kollár et al. [16] examined a dispersed water droplet two-phase flow in an icing wind tunnel. The gravity effects of large droplet sizes and droplet collisions were reported. The results indicated that the liquid water content accumulated in the bottom half of the wind tunnel for large droplets and a low air speed. The droplet size distribution near the spray nozzle outlet was different than the test section, due to the long trajectories of droplet motion. Phase change of supercooled droplets to ice, mass transfer with evaporation and sublimation were studied experimentally by Strub et al. [17]. Visualization of the droplet crystallization was observed and close agreement was achieved with predictive modeling.

These past studies indicate that a wide diversity of methods and configurations of forced convection with water droplets have been studied elsewhere. In particular cases, experimental methods have been developed to gain additional insight into the effects of water droplets. Jia and Qiu [18] investigated the dynamics of droplets and heat transfer in spray cooling problems, including a heating system, spray system, and droplet characterization system. Laser phase-Doppler anemometry with a dual-mechanism-scattering model was used to obtain the diameter of water droplets. A hollow copper cylinder with a cartridge heater and K-type thermocouple were used to determine the temperature and heat flux. A multinozzle spray system range with mass fluxes from 0.156 to 1.20 kg/m^2 supplied the water droplets. The results showed that the critical heat flux (CHF) can be avoided through water droplet cooling. Sawyer et al. [19] studied a horizontal, upward facing flat surface impacted by a stream of water droplets to obtain the effect of the droplet diameter and collision velocity on the critical heat flux. The CHF was expressed as a function of the Weber and Strouhal numbers of the impacting droplets.

Chen et al. [20] used a copper cylinder head with four 500 W cartridge heaters to investigate the impact of spray parameters on the CHF and heat transfer coefficient. The outcome showed that the mean droplet velocity and mean droplet flux had the most significant effect on CHF and heat transfer coefficient. The CHF and heat transfer coefficient increased at higher mean droplet velocities. The temperature transition of freezing droplets in a subzero airstream from the junction of a thermocouple and freezing time of a droplet were presented by Hindmarsh et al. [21]. Past studies have used various methods to measure coefficients of convective heat transfer from cylinders, airfoils, and other configurations in crossflow conditions. In this article, thermocouples embedded within a hollow airfoil (heated internally and cooled externally) will be used to study convective heat transfer with impinging droplets. One-dimensional heat conduction within the thin airfoil surface allows the temperature difference across the surface to give a close approximation of the Fourier conduction flux, which balances the convective heat flux in steady-state conditions. Water droplets are injected into the wind tunnel by a spray bar with an adjustable flow meter. Experimental data will be presented in terms of a Nusselt number correlation and multiphase Reynolds parameter. Measured data will be presented at varying Reynolds numbers, liquid water content, and surface positions.

II. Experimental Procedure

The forced convection experiments consist of a NACA-63421 airfoil in a refrigerated wind tunnel (see Fig. 1). The test section is a square duct, 91.6 cm in width and 91.6 cm in height. The wall of the test section is transparent, so that observations and photographs can be readily obtained. The airfoil is mounted horizontally within the tunnel. The velocity within the wind tunnel reaches up to 42 m/s at temperatures down to −35°C. The velocity is adjusted through an electrical control panel by varying the frequency of the motor, which drives the wind-tunnel fan.

Further details regarding the wind-tunnel setup and associated instrumentation were documented previously [22]. In this article, a prototype airfoil of a wind turbine blade or aircraft wing was fabricated for the experimental studies. A three-dimensional scanner was used to obtain the NACA profile representation of the airfoil, which was digitized with Geomagic Studio software. The airfoil center is hollow to reduce the weight. Figure 2 shows the front view and chord of the airfoil. The airfoil chord, span, and thickness are 500, 187.5, and 100 mm, respectively. Three sections of airfoil (each with a 62.5 mm span) were installed side by side to give a total span of 187.5 mm. The airfoil is fabricated with fiberglass and mounted in an aluminum frame inside the test section of the wind tunnel. The thickness of the airfoil fiberglass wall is 3 mm. T-type thermocouples are embedded at both inner and outer edges of the airfoil surface. The thermocouple junctions are mounted flush with each surface at several positions around the airfoil (see Fig. 2b). All thermocouple wires are gathered internally within the hollow section of the airfoil. Electrical heater strips are installed along the inner edges of the airfoil. The dimensions of the heating strips are 40 mm in width and 880 mm in length. The operating voltage of the heating strip is 120 V and the power input is set to 500 W for these experiments. The heater can be adjusted by a variable transformer over a range of voltages from 0 to 120 V. The heater strips are fastened to the inside of the airfoil with double-sided adhesive tape, after thermocouples are installed.

This paper focuses on the effects of droplet impact on convective heat transfer from the airfoil. To study these droplet effects, a spray system was constructed and installed upstream of the test section. Droplet emission from every nozzle was calibrated by controlling the atomizing air flow. Calibrating the mass flow to each nozzle required adjustment of the valves until a uniform flow was obtained. Droplets were emitted conically from the spray bar in parallel streams, which

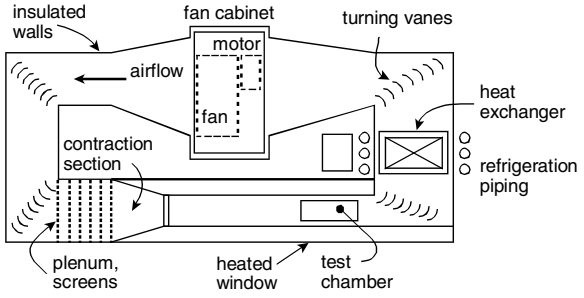

Fig. 1 Top view of refrigerated wind tunnel at the University of Manitoba.

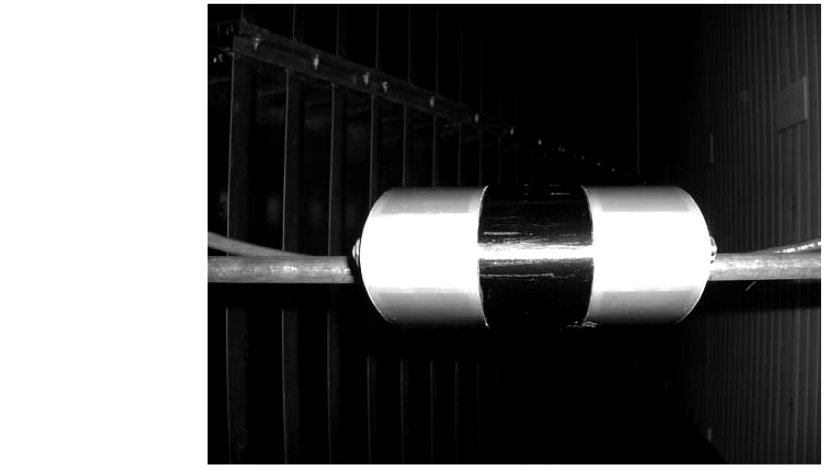

a)

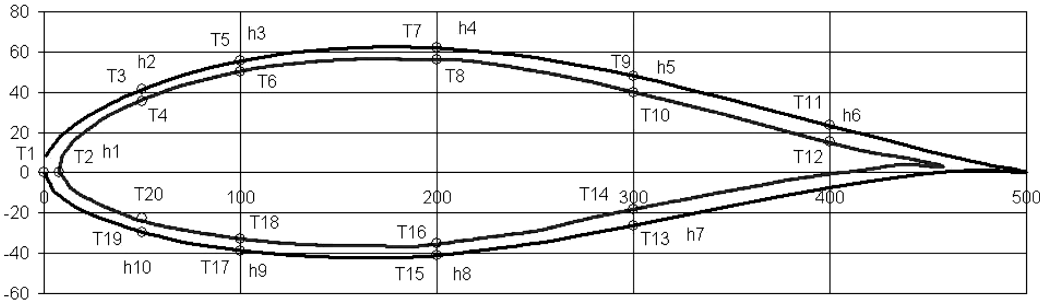

b)

Fig. 2 NACA-63421 airfoil a) in the test section with b) thermocouple locations (dimensions in millimeters).

overlapped to create a uniform droplet cloud that impacted on the airfoil surface.

A direct-reading temperature sensor was used to measure the temperature of the reference junction for cold-junction compensation. T-type thermocouples were used in a differential connection mode. The measurement system is controlled by a Labview software program. The experiment uses a total of 25 thermocouples mounted at various locations within the airfoil (see Fig. 2b), including 22 thermocouples installed along the inner and outer surfaces of the airfoil. Temperature differences between inner and outer surfaces are measured at 11 different locations. A thermocouple is inserted in the midplane of the wind tunnel. The thickness of the airfoil is very thin (3 mm) compared with the chord (500 mm) and span (62.5 mm), and so heat transfer is predominantly one-dimensional across the wall of the airfoil. Under steady-state conditions, the heat supplied by the heater is passed through the airfoil wall and transferred to the cold airstream by convection across the airfoil. Heat conduction through the airfoil is determined from thermocouple measurements within the wall, not the supply of heat input to the wall from the heater, which could be erroneous because of losses through the back side of the heater.

The rate of convective heat transfer from the airfoil is determined by

$$q_{\text{con}} = h(T_\infty - T_o) \tag{1}$$

which can be rearranged to give

$$h = \frac{q_{\text{con}}}{T_\infty - T_o} \tag{2}$$

Heater strips below the airfoil surface provide a source of heat input, which is transported through the thin airfoil surface by conduction, then convection to the external airstream. Heat conduction perpendicular to the surface is much larger than lateral heat conduction, due to the high temperature difference across the thin surface. Thus, the perpendicular Fourier heat flux balances the rate of convective heat transfer to the surrounding airstream, i.e.,

$$q_{\text{con}} = q_{\text{cd}} = \frac{k(T_{\text{in}} - T_o)}{\delta} \tag{3}$$

Substituting Eq. (2) into Eq. (3), the resulting heat transfer coefficient can be expressed in the following manner:

$$h = \frac{k(T_{\text{in}} - T_o)}{\delta(T_\infty - T_o)} \tag{4}$$

The average coefficient was obtained from spatial averaging around the airfoil.

$$\bar{h} = \frac{1}{s}\int_s h\,\mathrm{d}x = \frac{1}{s}\sum_i^{11} h_i \Delta s_i \tag{5}$$

Then, the average Nusselt number becomes

$$\overline{Nu} = \frac{\bar{h}c}{k_{\text{air}}} \tag{6}$$

The experimental uncertainty of the measured Nusselt number depends on the uncertainty of the local heat transfer coefficient, airfoil chord, thermal conductivity, and geometrical factors. The local heat transfer coefficient depends on the temperature difference between the surface and freestream, as well as the net convective heat loss for each test case. In the next section, a detailed analysis of measurement uncertainties will be presented.

III. Analysis of Measurement Uncertainties

The method of Kline and McClintock [23] was used to determine the measurement uncertainties in the heat transfer experiments. In the experiments, the parameters T_o, T_i, T_∞, and δ were measured. The

total uncertainty U_h includes a precision uncertainty P_h and B_h (precision and bias limit for each variable and parameter contribution to the uncertainty).

$$U_h = \sqrt{P_h^2 + B_h^2} \tag{7}$$

The precision contribution can be calculated with the following propagation equation, which extends the method of Kline and McClintock [23] to the current problem parameters as follows.

$$P_h^2 = \left(\frac{\partial h}{\partial T_{\text{in}}}\right)^2 P_{Ti}^2 + \left(\frac{\partial h}{\partial T_o}\right)^2 P_{To}^2 + \left(\frac{\partial h}{\partial T_\infty}\right)^2 P_{T\infty}^2 + \left(\frac{\partial h}{\partial \delta}\right)^2 P_\delta^2 + \left(\frac{\partial h}{\partial k}\right)^2 P_k^2 \tag{8}$$

Using Eq. (4) to evaluate the derivatives and defining $\Delta T_1 = T_{\text{in}} - T_o$ and $\Delta T_2 = T_o - T_\infty$, it can be shown that Eq. (8) yields

$$\left(\frac{P_h}{h}\right)^2 = \left(\frac{P_{Ti}}{\Delta T_1}\right)^2 + \left(\frac{P_{To}}{\Delta T_2}\right)^2 + \left(\frac{P_{T\infty}}{\Delta T_2}\right)^2 + \left(\frac{P_\delta}{\delta}\right)^2 + \left(\frac{P_k}{k}\right)^2 \tag{9}$$

Using a similar procedure, it can be shown that the following result is obtained for the bias contribution,

$$\left(\frac{B_h}{h}\right)^2 = \frac{B_{Ti}^2}{\Delta T_1^2} + \left(\frac{1}{\Delta T_1} + \frac{1}{\Delta T_2}\right)^2 B_{To}^2 - 2\left(\frac{1}{\Delta T_1^2} + \frac{1}{\Delta T_1 \Delta T_2}\right) B'_{To} B'_{Ti} + \frac{2}{\Delta T_1 \Delta T_2} B'_{T\infty} B'_{Ti} - 2\left(\frac{1}{\Delta T_2^2} + \frac{1}{\Delta T_1 \Delta T_2}\right) B'_{To} B'_{T\infty} + \frac{B_{T\infty}^2}{\Delta T_2^2} + \frac{B_k^2}{k^2} + \frac{B_\delta^2}{\delta^2} \tag{10}$$

where B'_{Ti}, B'_{To}, and $B'_{T\infty}$ are the portions of B_{Ti}, B_{To}, and $B_{T\infty}$, respectively, which arise from an identical error source, and so they are assumed to be perfectly correlated. The bias contribution to the uncertainty becomes

$$\left(\frac{B_h}{h}\right)^2 = \frac{B_k^2}{k^2} + \frac{B_\delta^2}{\delta^2} \tag{11}$$

Then, the total uncertainty of the heat transfer coefficient becomes

$$\frac{U_h}{h} = \sqrt{\left(\frac{P_h}{h}\right)^2 + \left(\frac{B_h}{h}\right)^2} \tag{12}$$

For the current experiments, $P_{Ti} = P_{To} = P_{T\infty} = 0.64$ K, $\Delta T_1 = 10.25$ K, $\Delta T_2 = 42.42$ K, $P_\delta = 0.095$ mm, $\delta = 2.999$ mm, and $B_\delta = 0.005$ mm. It was assumed that $P_h/k = 0$ and $B_k/k = 0$. Using these parameters, the uncertainty of the heat transfer coefficient becomes $U_h/h = 7.32\%$.

The Nusselt number is $\overline{Nu} = \bar{h}c/k$, and so its total uncertainty can be expressed in the following manner:

$$\frac{U_{\overline{\text{Nu}}}}{\overline{Nu}} = \sqrt{\left(\frac{P_{\overline{\text{Nu}}}}{\overline{Nu}}\right)^2 + \left(\frac{B_{\overline{\text{Nu}}}}{\overline{Nu}}\right)^2} = \sqrt{\left(\frac{U_h}{h}\right)^2 + \left(\frac{B_c}{c}\right)^2 + \left(\frac{B_k}{k}\right)^2} = 7.25\% \tag{13}$$

It can be shown that the measurement uncertainty of the average freestream velocity is $U_u/u = 0.397\%$. Also, the uncertainties of the tabulated density of air and manometer fluid for the pitot tube measurements of velocity are $U_{\rho_l}/\rho_l = U_{\rho_{\text{air}}}/\rho_{\text{air}} = 0.5\%$. As a result, the uncertainty of the measured Reynolds number is 0.818% based on the uncertainty of velocity, density of air, viscosity, and bias of chord length. This measurement uncertainty of the Reynolds number indirectly affects the uncertainty of Nu through the heat transfer coefficient, which depends on the air velocity and other parameters. The resulting measurement uncertainty of the Nusselt number was 7.34%. In the next section, results will be presented for the Nusselt number, which will be subject to the quoted uncertainties described in this section.

IV. Results and Discussion

Experimental results will be presented for convective heat transfer from a NACA-63421 airfoil. The Reynolds number will be varied by changing the air velocity in the icing tunnel, air viscosity, and thermal diffusivity (by changing the air temperatures). The liquid water content is also varied through different spray flow conditions. Within the refrigerated wind tunnel, air temperatures are varied between 20 and −30°C. The liquid water content ranges from 0 to 12 gal/h (about 45 l/h). Data were collected over a range of temperatures and liquid water contents that yielded uniform normalizations of the Nusselt numbers. For example, normalized data collapsed onto a single curve fit at different temperatures, which indicated consistency and provided useful verification that experimental data were collected accurately.

Extensive effort was taken to ensure uniformity of the droplet distribution, as best as possible. Atomizing nozzles were adjusted iteratively with the air and water streams, simultaneously, to improve uniformity. This was time consuming because they affected each other. Also, particle imaging velocimetry was used to analyze the uniformity of the droplet distribution at each step. Furthermore, icing patterns were observed on the airfoil and the uniformity of ice buildup provided another indication of the droplet distribution uniformity. These efforts and others were taken to provide as uniform a droplet distribution as possible. From the manufacturer's specifications of the spray nozzles, the droplet size is very small (order of 100 μm). At the nozzle exit, droplet ejection is air-assisted because the airstream drives the emission from the nozzle, rather than ejection at a particular velocity, and so the droplet velocity is close to the airstream velocity. Because of the atomizing nozzles with a high air pressure of 55 psi and lower water pressure of 35 psi, the resulting droplet sizes are controlled accurately for a very small size. The air atomizing nozzles can produce a reliable spray pattern with water mean droplet diameters ranging between 1000 and 10 μm.

A transition Reynolds number of $Re_c \geq 6 \times 10^5$ characterizes transition to turbulence of the boundary layer over the airfoil. This transition point also occurs for a flat plate and cylinder, although the transition number for a cylinder in crossflow occurs at $Re_D = 2 \times 10^5$. Because of these similarities, experimental data will be correlated against the following functional form of Nusselt number, which is equivalent to the Hilpert correlation for a cylinder in crossflow [7],

$$\overline{Nu} = cRe^m Pr^{1/3} \tag{14}$$

The liquid water content has substantial effects on the heat transfer coefficient. Figure 3 illustrates the measured data at different values of the liquid water content, together with a correlated curve fit of experimental data without water droplets, which was derived by conducting the experiments at the same operating temperature, but with the spray nozzles closed. In Fig. 3, the solid curves represent empirical correlations without droplets, whereas the markers correspond to measured data with droplets. The same Reynolds number is used in each case for consistency purposes. The experimental data indicate that the average Nusselt number rises about 26.7 and 27.4%, respectively, for $Re_c < 6 \times 10^5$ and $Re_c \geq 6 \times 10^5$ when water droplets are introduced into the airstream. Thus, impinging droplets enhance the rate of heat exchange between the surface and airstream. Impinging droplets enhance fluid mixing along the wall, thereby increasing the convective heat exchange and Nusselt number.

Inspecting the measured data (with droplets) closely in Fig. 3, it can be observed that no distinct trend can be observed with varying liquid water content. In other words, the Nusselt number is higher at low Reynolds numbers for the case of smaller liquid water content. However, it is lower at the highest Reynolds number in Fig. 3b. Furthermore, each data point is associated with a different liquid water content, which is not labeled in the figure (only broadly within

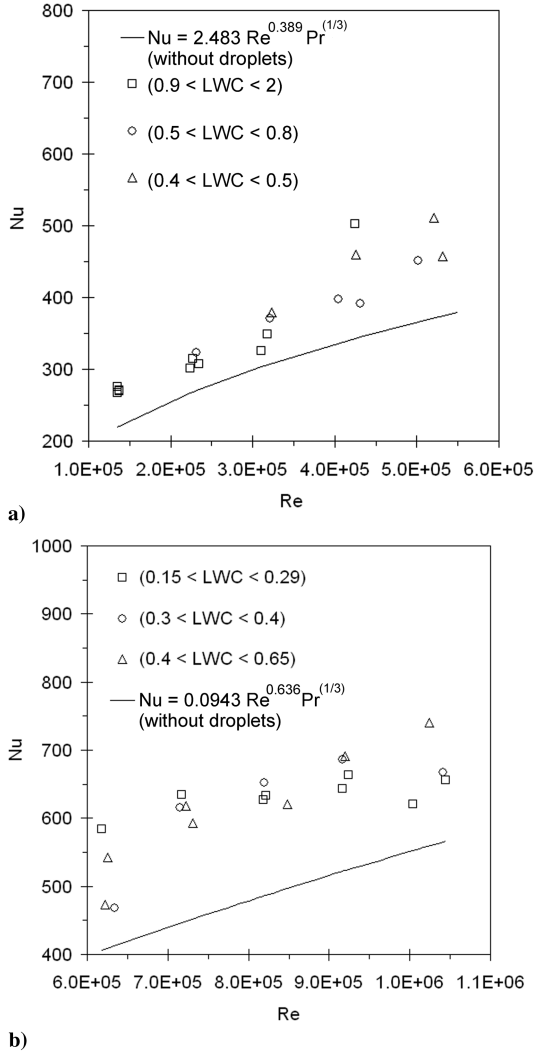

Fig. 3 ***Nu*** **correlation at a) low and b) high Reynolds numbers.**

a range of liquid water content values). As a result, it would be useful to normalize the data in a suitable manner, which reduces dependence to a single parameter involving both the Reynolds number and liquid water content.

To achieve this objective, experimental data were first correlated against the Reynolds number without droplets in the airstream. A modified Hilpert correlation, Eq. (14), was used in a curve fit of measured data over a range of Reynolds numbers. The coefficients (c and m) were determined based on a least-squares curve fit of measured data. It was observed that all data points lied close to a single normalized curve for each Prandtl number investigated, which was found independently at different temperatures. This close agreement provided useful verification that measurements exhibit consistent behavior under appropriate normalization at varying Reynolds numbers. For low Reynolds numbers ($Re \leq 6 \times 10^5$) and high numbers ($Re > 6 \times 10^5$), respectively, the following correlations were obtained:

$$\overline{Nu} = 2.483 Re^{0.389} Pr^{1/3} \qquad (\text{for } Re \leq 6 \times 10^5) \tag{15}$$

$$\overline{Nu} = 0.0943 Re^{0.636} Pr^{1/3} \qquad (\text{for } Re > 6 \times 10^5) \tag{16}$$

The standard deviation between experimental data and the correlation coefficient for the best curve fit was 8.25 and 11.9 for the Nusselt number at low and high Reynolds numbers, respectively. Also, R^2 was 0.8517 and 0.8149, separately.

Extensions to cases with impinging droplets were made based on these correlations. It was determined that a multiphase Reynolds parameter, $Re_m = Re(1 + W)$, leads to a promising method of normalizing experimental data. In other words, the Nusselt number correlation was established as follows:

$$\overline{Nu} = c[Re(1 + W)]^m Pr^{1/3} \tag{17}$$

$$W = \frac{\text{LWC}}{\text{LWC}_0} \tag{18}$$

where LWC_0 refers to a reference value of the liquid water content. By selecting the reference value equal to one-fourth of the maximum water content in air at the average temperature, it was observed that the same Nusselt number correlation could be used for both single-phase (without droplets) and two-phase flows (with droplets), provided the Reynolds number is replaced with the multiphase Reynolds parameter. At the average temperature of -0.16°C for the low-speed set of experiments, the maximum water content in air is 4.98 g/m^3, and so the reference water content was taken as 1.25 g/m^3. The average temperature is -4.55°C for the higher speed set of experiments, and so the maximum liquid water content at this temperature is 3.69 g/m^3 and the reference liquid water content becomes 0.92 g/m^3.

As a result, the correlations of Nusselt number with respect to the multiphase Reynolds parameter become

$$\overline{Nu} = 2.483[Re(1 + W)]^{0.389} Pr^{1/3} \qquad (\text{for } Re(1 + W) \leq 6 \times 10^5) \tag{19}$$

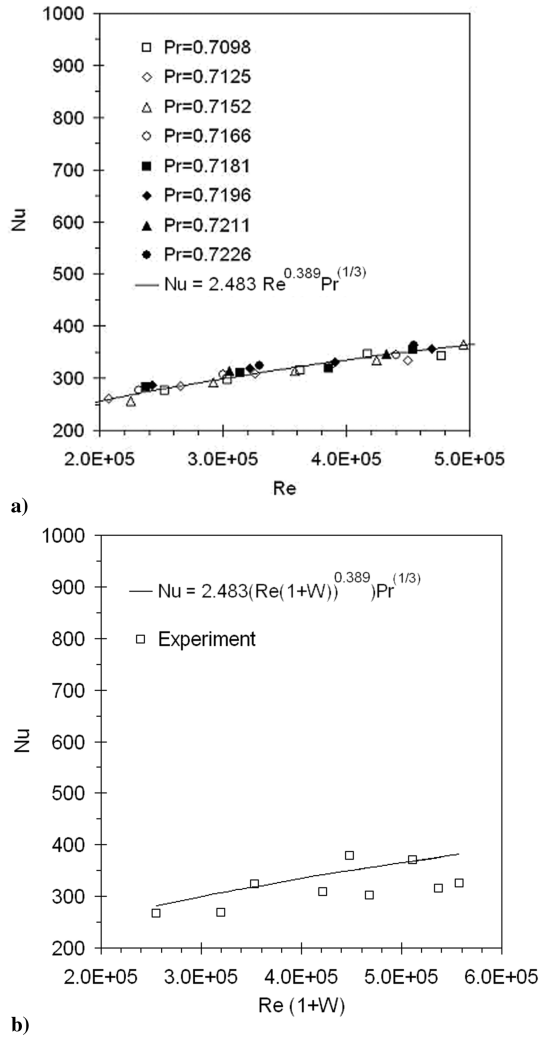

Fig. 4 Predicted and measured ***Nu*** **a) without and b) with droplets for** $Re(1 + W) < 600,000$.

$$\overline{Nu} = 0.0943[Re(1+W)]^{0.636}Pr^{1/3} \quad (\text{for } Re(1+W) > 6\times 10^5) \tag{20}$$

The experimental data show close agreement with these correlations in Figs. 4–6. This close agreement provides useful verification that measurements exhibit consistent behavior under appropriate normalization at varying Reynolds numbers. Without the multiphase Reynolds parameter, a consistent trend could not be observed with the data. But the definition of $Re(1+W)$ allows effective normalization of measured data and it incorporates effects of both Reynolds number and LWC, thereby reducing the number of independent variables in plotted figures.

In Fig. 4, the measured Nusselt number is shown without droplets (Fig. 4a) and with droplets (Fig. 4b) at $Re \le 6\times 10^5$. When using the single-phase Reynolds parameter in Fig. 4a and multiphase parameter in Fig. 4b, it can be observed that very similar trends are obtained. Such close similarity would not be achieved without the new multiphase Reynolds parameter. Values at different Prandtl numbers in Fig. 4a are obtained through varying temperatures within the wind tunnel, which alter the dynamic viscosity and thermal diffusivity of the airstream. Analogous trends and close proximity between correlated data with and without droplets can be observed in Fig. 4b at higher Reynolds numbers ($Re \le 6\times 10^5$). The multiphase Reynolds parameter is shown to provide normalization against single-phase correlations over a wide range of Reynolds numbers.

Several key differences should be noted between Figs. 3–5. In Fig. 3, measured data are shown at different values of the liquid water content (two-phase flow with droplets), whereas Figs. 4a and 5a show Nusselt numbers at varying temperatures and Prandlt numbers (without droplets). The measured data in Figs. 4a and 5a were used to develop the empirical correlations in Fig. 3. Also, Figs. 4b and 5b plot Nusselt numbers against the multiphase Reynolds parameter, whereas Fig. 3 plots the Nusselt number against the conventional, single-phase Reynolds number (without droplets). The results in Figs. 4b and 5b are nearly independent of Prandtl number because the temperature range and variations of Prandtl number are small. The data are the same as results in Figs. 3a and 3b, except that it is normalized by LWC_0 and plotted against the multiphase Reynolds parameter, rather than the conventional single-phase Reynolds number. The number of measured data points in Figs. 3–5 is different because the Reynolds number on the horizontal axis is different, thereby affecting the number of data points lying within a given range.

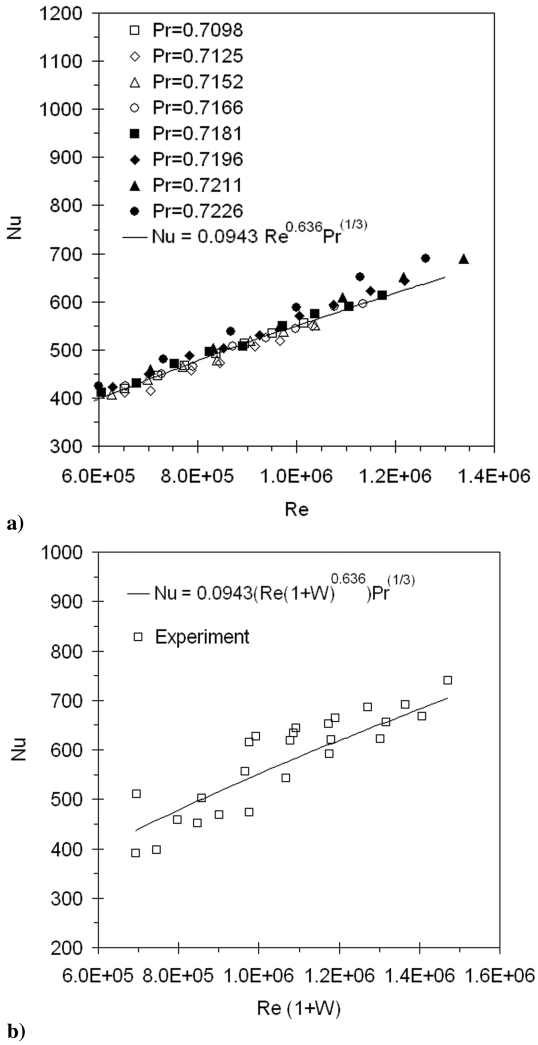

Fig. 5 Predicted and measured *Nu* a) without and b) with droplets for $Re(1+W) < 600,000$.

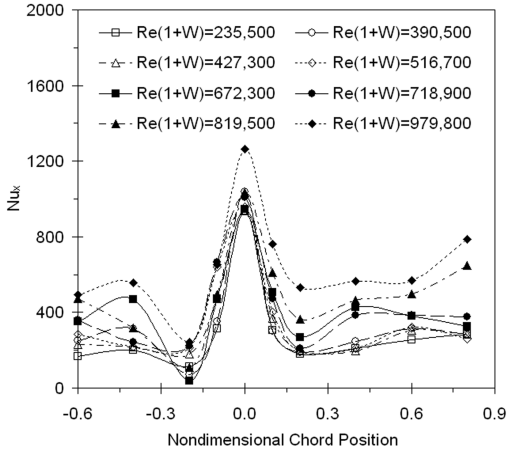

Fig. 6 Local Nusselt number at varying Reynolds numbers.

Figure 6 shows the local Nusselt numbers at different positions and multiphase Reynolds numbers. The stagnation point is $x/C = 0$. The Nusselt number decreases dramatically after the stagnation point, due to the rapidly thickening boundary layer along the top and bottom surfaces. It falls to a lowest point at the position of $0.2c$ along the chord of the airfoil, after which it increases. Although both surfaces of the airfoil have the same trends near the leading edge of the airfoil, the lowest value of Nu_x occurs along the bottom surface. The airfoil is nonsymmetric, and so a different streamline pattern occurs along the bottom surface. The surface would have the same local Nusselt number as the top surface, if the airfoil was symmetric in shape and orientation, with respect to the freestream. The local Nusselt number for the NACA-63421 airfoil has different trends below and above the stagnation point, due to its nonsymmetrical profile. On the airfoil, the thickness of laminar boundary layer increases as x increases from the leading edge to the trailing edge. Afterward, boundary layer transition occurs and the boundary layer becomes turbulent. In the laminar region, the heat transfer coefficient decreases as the thickness of the boundary layer increases. As the boundary layer becomes turbulent, the heat transfer coefficient increases. These trends can be clearly seen in Fig. 6.

V. Conclusions

This article has presented an experimental study of heat transfer coefficients for forced convection with droplet impact on a NACA-63421 airfoil. Wind-tunnel measurements of the convection coefficients were obtained for varying Reynolds numbers and LWC values ranging between 0 and 2 g/m^3. The experimental data were correlated with respect to the Nusselt number and newly defined multiphase Reynolds number. Both average and spatial variations of the heat transfer coefficients were nondimensionalized through modifications of a Hilpert correlation for cylinders in crossflow. The liquid water content was normalized by $W = LWC/LWC_0$, where the reference value was $LWC_0 = 0.92$ for LWC values less than

1 g/m^3 and $LWC_0 = 1.25$ for LWC values between 1 and 2 g/m^3. It was shown that the functional form of the Hilpert correlation can effectively accommodate measured data for the NACA airfoil over a range of Reynolds numbers. An uncertainty analysis was performed to give an experimental uncertainty of 7.34% for the measured Nusselt numbers.

Acknowledgments

Financial support from the Natural Sciences and Engineering Research Council of Canada, Manitoba Hydro, and the Canada Foundation for Innovation are gratefully acknowledged.

References

[1] Messinger, B. L., "Equilibrium Temperature of an Unheated Icing Surface as a Function of Air Speed," *Journal of the Aeronautical Sciences*, Vol. 20, 1953, pp. 29–42.

[2] Naterer, G. F., "Reduced Flow of a Metastable Layer at a Two-Phase Limit," *AIAA Journal*, Vol. 42, No. 5, 2004, pp. 980–987.

[3] Naterer, G. F., *Heat Transfer in Single and Multiphase Systems*, CRC Press, Boca Raton, FL, 2003.

[4] Al-Khalil, K. M., Keith, T. G., Jr., and De Witt, K. J., "New Concept in Runback Water Modeling for Anti-Iced Aircraft Surface," *Journal of Aircraft*, Vol. 30, No. 1, 1993, pp. 41–49.

[5] Papadakis, M., Elangovan, R., Freund, G. A., and Breer, M. D., "Water Droplet Impingement on Airfoils and Aircraft Engine Inlets for Icing Analysis," *Journal of Aircraft*, Vol. 28, No. 3, 1991, pp. 165–174.

[6] Naterer, G. F., "Dispersed Multiphase Flow with Air-Driven Runback of a Liquid Layer at a Moving Boundary," *International Journal of Multiphase Flow*, Vol. 29, No. 12, 2003, pp. 1833–1856.

[7] Incropera, F. P., and deWitt, D. P., *Fundamentals of Heat and Mass Transfer*, 4th ed., Wiley, New York, 1996, Chap. 7.

[8] Fortin, G., Laforte, J. L., and Ilinca, A., "Heat and Mass Transfer During Ice Accretion on Aircraft Wings with an Improved Roughness Model," *International Journal of Thermal Sciences*, Vol. 45, 2006, pp. 595–606.

[9] Naterer, G. F., "Temperature Gradient in the Unfrozen Liquid Layer for Multiphase Energy Balance with Incoming Droplets," *Journal of Heat Transfer*, Vol. 125, No. 1, 2003, pp. 186–189.

[10] Fu, P., Farzaneh, M., and Bouchard, G., "Two-Dimensional Modelling of the Ice Accretion Process on Transmission Line Wires and Cables," *Cold Regions Science and Technology*, Vol. 46, No. 3, Nov. 2006, pp. 132–146.

[11] Ge, Y., and Fan, L. S., "3-D Modeling of the Dynamics and Heat Transfer Characteristics of Subcooled Droplet Impact on a Surface with Film Boiling," *International Journal of Heat and Mass Transfer*, Vol. 49, 2006, pp. 4231–4249.

[12] Naterer, G. F., and Camberos, J. A., "Entropy and the Second Law in Fluid Flow and Heat Transfer Simulation," *Journal of Thermophysics and Heat Transfer*, Vol. 17, No. 3, 2003, pp. 360–371.

[13] Hedrih, K., Babović, V., and Šarković, D., "Auxiliary Size Distribution Model for the Ultrasonically Produced Water Droplets," *Experimental Thermal and Fluid Science*, Vol. 30, 2006, pp. 559–564.

[14] Fuchs, W., and Schickel, K. P., "Aircraft Icing in Visual Meterological Conditions Below Low Stratus Clouds," *Atmospheric Research*, Vol. 36, 1995, pp. 339–345.

[15] Yoon, S. S., DesJardin, P. E., Presser, C., Hewson, J. C., and Avedisian, C. T., "Numerical Modeling and Experimental Measurements of Water Spray Impact and Transport over a Cylinder," *International Journal of Multiphase Flow*, Vol. 32, 2006, pp. 132–157.

[16] Kollár, L. E., Farzaneh, M., and Karev, A. R., "Modeling Droplet Collision and Coalescence in an Icing Wind Tunnel and the Influence of These Processes on Droplet Size Distribution," *International Journal of Multiphase Flow*, Vol. 31, 2005, pp. 69–92.

[17] Strub, M., Jabbour, O., Strub, F., and Bédécarrats, J. P., "Experimental Study and Modeling of the Crystallization of a Water Droplet," *International Journal of Refrigeration*, Vol. 26, 2003, pp. 59–68.

[18] Jia, W., and Qiu, H. H., "Experimental Investigation of Droplet Dynamics and Heat Transfer in Spray Cooling," *Experimental Thermal and Fluid Science*, Vol. 27, 2003, pp. 829–838.

[19] Sawyer, M. L., Jeter, S. M., and Abdel-Khaliks, S. I., "Critical Heat Flux Correlation for Droplet Impact Cooling," *International Journal of Heat and Mass Transfer*, Vol. 40, No. 9, 1997, pp. 2123–2131.

[20] Chen, R. H., Chow, L. C., and Navedo, J. E., "Effects of Spray Characteristics on Critical Heat Flux in Subcooled Water Spray Cooling," *International Journal of Heat and Mass Transfer*, Vol. 45, 2002, pp. 4033–4043.

[21] Hindmarsh, J. P., Russell, A. B., and Chen, X. D., "Experimental and Numerical Analysis of the Temperature Transition of a Suspended Freezing Water Droplet," *International Journal of Heat and Mass Transfer*, Vol. 46, 2003, pp. 1199–1213.

[22] Naterer, G. F., Popplewell, N., Barrett, W., Anderson, J., Faraci, E., McCartney, D., and Lehmann, W., "Experimental Facility for New Hybrid Ice/Spray Flow Tunnel with Laser Based Droplet Measurement," *AIAA 32nd Fluid Dynamics Conference, St. Louis, Missouri, 24– 27 June 2002*, AIAA Paper 2002-2867, 2002.

[23] Kline, S. J., and McClintock, F. A., "Describing Uncertainties in Single-Sample Experiments," *Mechanical Engineering*, Vol. 75, 1953, pp. 3–8.